OECD MCCI Project

Small-Scale Water Ingression and Crust Strength Tests (SSWICS)

SSWICS-2 Test Data Report: Thermal Hydraulic Results

Rev. 0 September 20, 2002

by:

S. Lomperski, M. T. Farmer, D. J. Kilsdonk, and R. W. Aeschlimann
Reactor Analysis and Engineering Division
Argonne National Laboratory
9700 S. Cass Avenue
Argonne, IL 60439 USA

S. Basu
Project Manager
U.S. Nuclear Regulatory Commission

Table of Contents

List of Plots

1. Introduction

The Melt Attack and Coolability Experiments (MACE) program at Argonne National Laboratory addressed the issue of the ability of water to cool and thermally stabilize a molten core/concrete interaction (MCCI) when the reactants are flooded from above. These tests provided data regarding the nature of corium interactions with concrete, the heat transfer rates from the melt to the overlying water pool, and the role of noncondensable gases in the mixing processes that contribute to melt quenching. However, due to the integral nature of these tests, several questions regarding the crust freezing behavior could not be adequately resolved. These questions include:

1) To what extent does water ingression into the crust increase the melt quench rate above the conduction-limited rate and how is this affected by melt composition and system pressure?
2) What is the fracture strength of the corium crust when subjected to a thermal-mechanical load and how does it depend upon the melt composition?

A series of separate-effects experiments are being conducted to address these issues. The first employs an apparatus designed to measure the quench rate of a pool of corium (~ϕ30 cm; up to 20 cm deep). The main parameter to be varied in these quench tests is the melt composition since it is thought to have a critical influence on the crust cracking behavior which, in turn, alters quench rate. The issue of crust strength will be addressed with a second apparatus designed to mechanically load the crust produced by the quench tests. This apparatus will measure the fracture strength of the crust while under a thermal load created by a heating element beneath the crust. The two apparatuses used to measure the melt quench rate and crust strength are jointly referred to as SSWICS (Small-Scale Water Ingression and Crust Strength).

This report describes results of the second water ingression test, designated SSWICS-2. The report includes a description of the test apparatus, the instrumentation used, plots of the recorded data, and some rudimentary data reduction to obtain an estimate of the heat flux from the corium to the overlying water pool.

2. System Description

2.1 Test Apparatus

The SSWICS reaction vessel (RV) has been designed to hold up to 100 kg of melt at an initial temperature of 2500^{o}C. The RV lower plenum consists of a 67.3 cm long, 45.7 cm (18") outer diameter carbon steel pipe (fig. 2.1). The pipe is insulated from the melt by a 6.4 cm thick layer of cast MgO. The selected pipe and insulation dimensions result in a melt diameter of 30.5 cm and a surface area of 730 cm^2. The melt depth at the maximum charge of 100 kg is about 20 cm.

The RV lower flange is insulated with a 6.4 cm thick slab of cast MgO that spans the entire inner diameter of the pipe. The MgO slab and sidewalls form the crucible containing the corium. This particular geometry was chosen to facilitate removal of the slab for the crust strength

measurement tests. Corium has a tendency to bond with the MgO insulation and this design allows one to pry the slab away from the MgO walls without damaging the crust.

The MgO slab lies beneath a 1.3 cm thick cast ZrO_2 plate. The ZrO_2 is added because of its exceptionally low thermal conductivity at high temperature (~1 W/m^{o}C, versus ~10 for MgO at 2000^{o}C). Despite its low thermal conductivity, the ZrO_2 is not used as the primary insulator to protect the flange because of its poor thermal shock resistance. To protect the cast ZrO_2 plate from the initial thermal shock following thermite ignition, a disk of low-density ZrO_2 board is set on top of the cast plate. This material is not structurally robust and serves as a sacrificial layer that absorbs the initial thermal shock of thermite ignition. Finally, a thin layer (0.25 mm) of tungsten is added in an effort to prevent the erosion of the ZrO_2 that is expected if the corium was allowed to come in direct contact with the low-density board.

The RV upper plenum consists of a second section of pipe lined with cast MgO. Three 10 cm pipes welded near the top of the vessel provide 1) a vent line for the initial surge of hot noncondensable gases generated by the thermite reaction, 2) a pressure relief line with a 6 bar rupture disk, and 3) an instrument flange for the absolute pressure transmitter that measures the reaction vessel pressure. Four 6 mm (¼") tubes serve as water inlets for melt quenching. A baffle is mounted below the upper flange and the water flow is directed towards the baffle to reduce the momentum of the fluid before it drops down onto the melt. The baffle is also intended to prevent water droplets from being carried up towards the condenser, which would adversely affect the heat flux measurement. A fourth 10 cm pipe welded to the top flange provides an outlet to carry steam from the quenching melt to four cooling coils. The water-cooled coils condense the steam, which is collected within a 200 cm high, 20 cm diameter condensate tank (CT). Figure 2.2 is a schematic that provides an overview of the entire SSWICS melt-quench facility.

2.2 Instrumentation

Instrumentation has been selected to provide all measurements necessary to determine the melt dryout heat flux. Tables 2.1 and 2.2 list the sensors and major valves, respectively.

The critical measurement for these tests is the steaming rate in the RV, which is found indirectly by measuring the rate of condensate collection in the CT. Two differential pressure sensors, PD1-CT and PD2-CT, are used to measure condensate inventory. A time domain reflectometer, which would measure water level, arrived shortly after this test was performed.

The remaining instrumentation provides supplementary information to further characterize the test conditions. The initial melt temperature is provided by two Type-C thermocouples located 20 mm above the bottom of the melt and 7.5 cm from the RV centerline (halfway to the MgO wall). A second pair of type-C thermocouples below the ZrO_2 board and near the bottom of the melt is used to detect the arrival of the quench front. The melt is considered quenched when the temperature at the base of the melt reaches the saturation temperature, and this is the basis for terminating the test. Figure 2.3 illustrates the thermocouple locations within the RV. The nomenclature used to identify the thermocouples is as follows: TIW (temperature at the inner wall of the MgO insulator, TM (temperature within the corium melt), H# (height above the

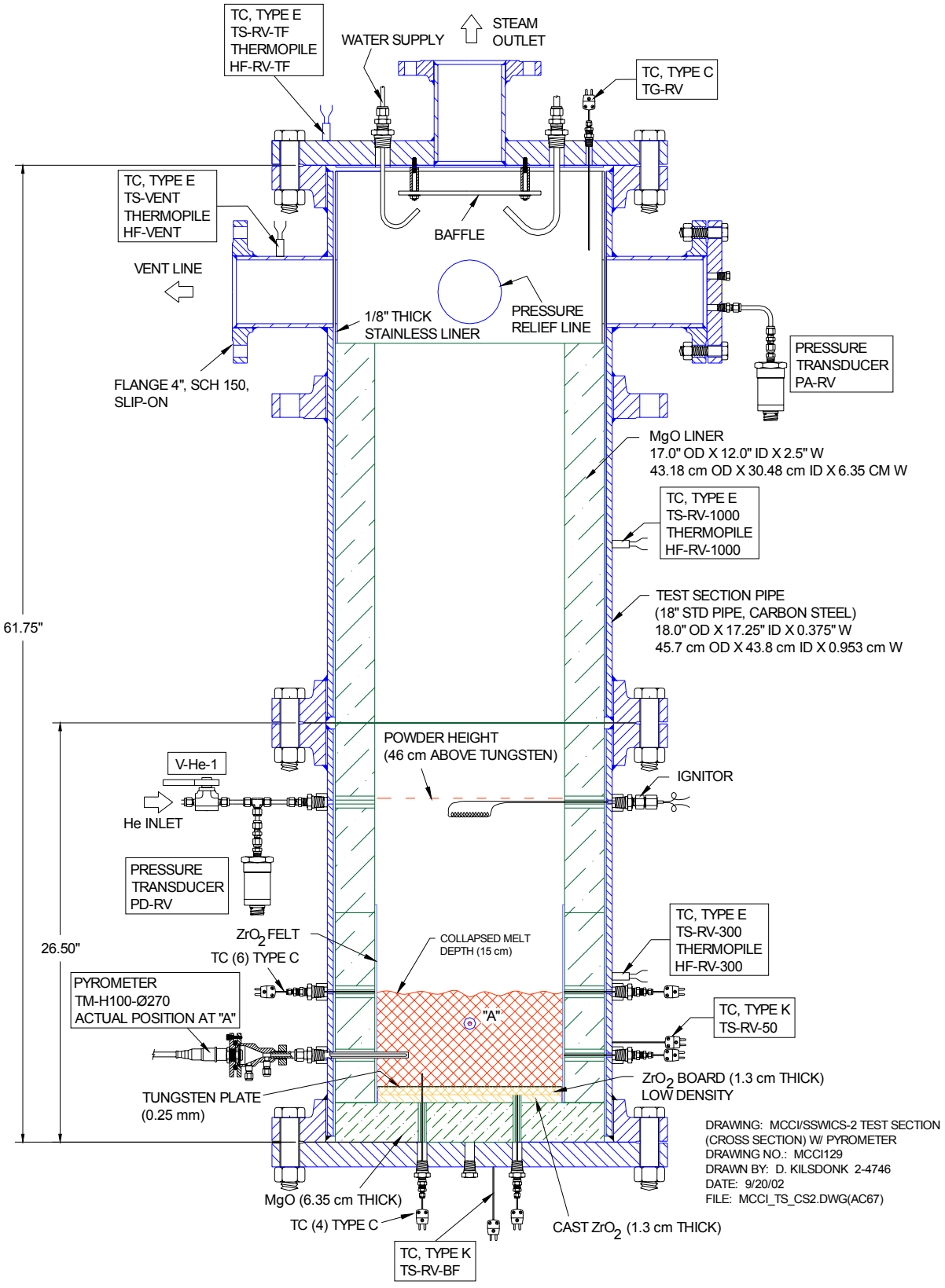

Figure 2.1 Side view of reaction vessel.

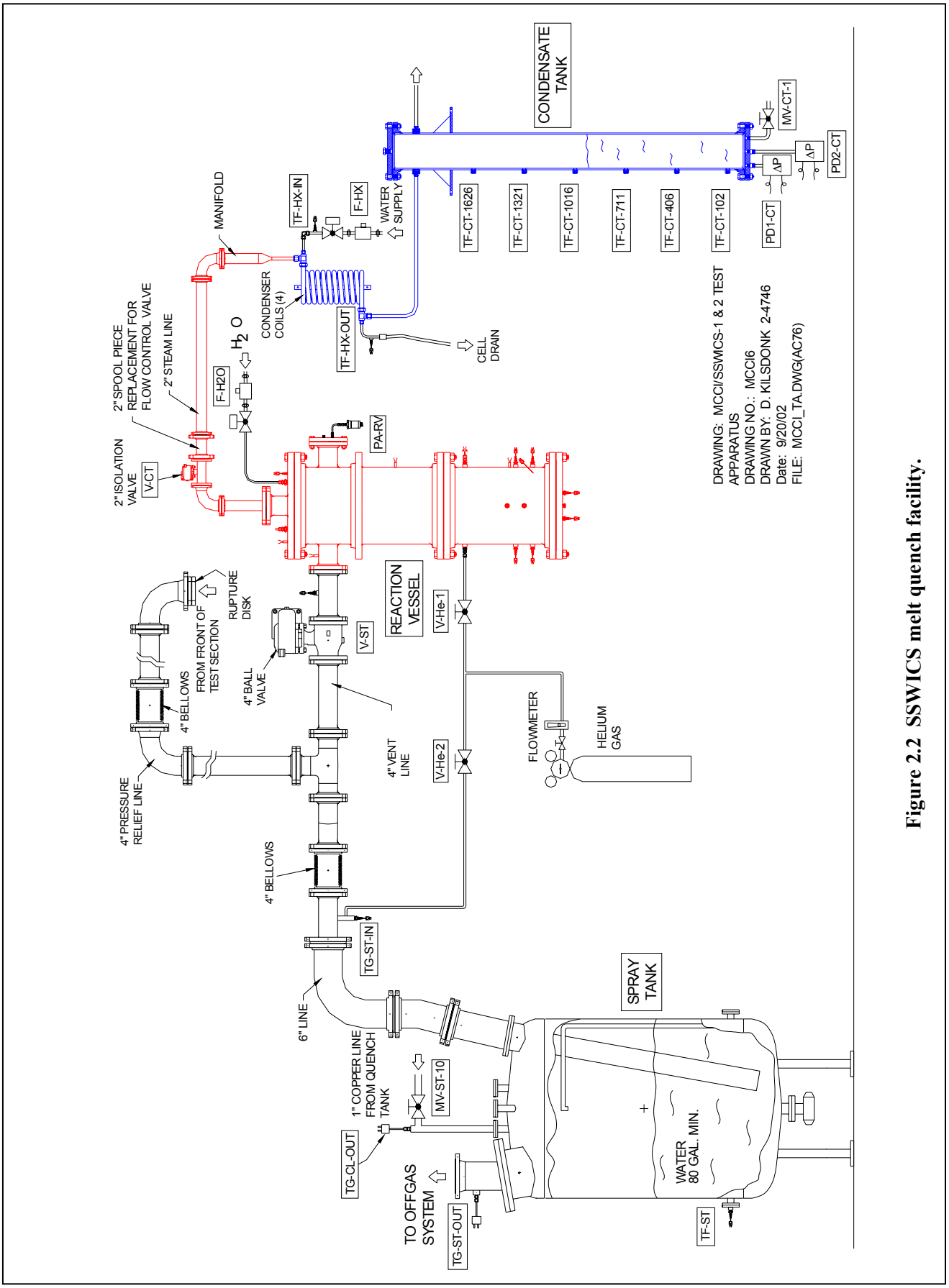

Figure 2.2 SSWICS melt quench facility.

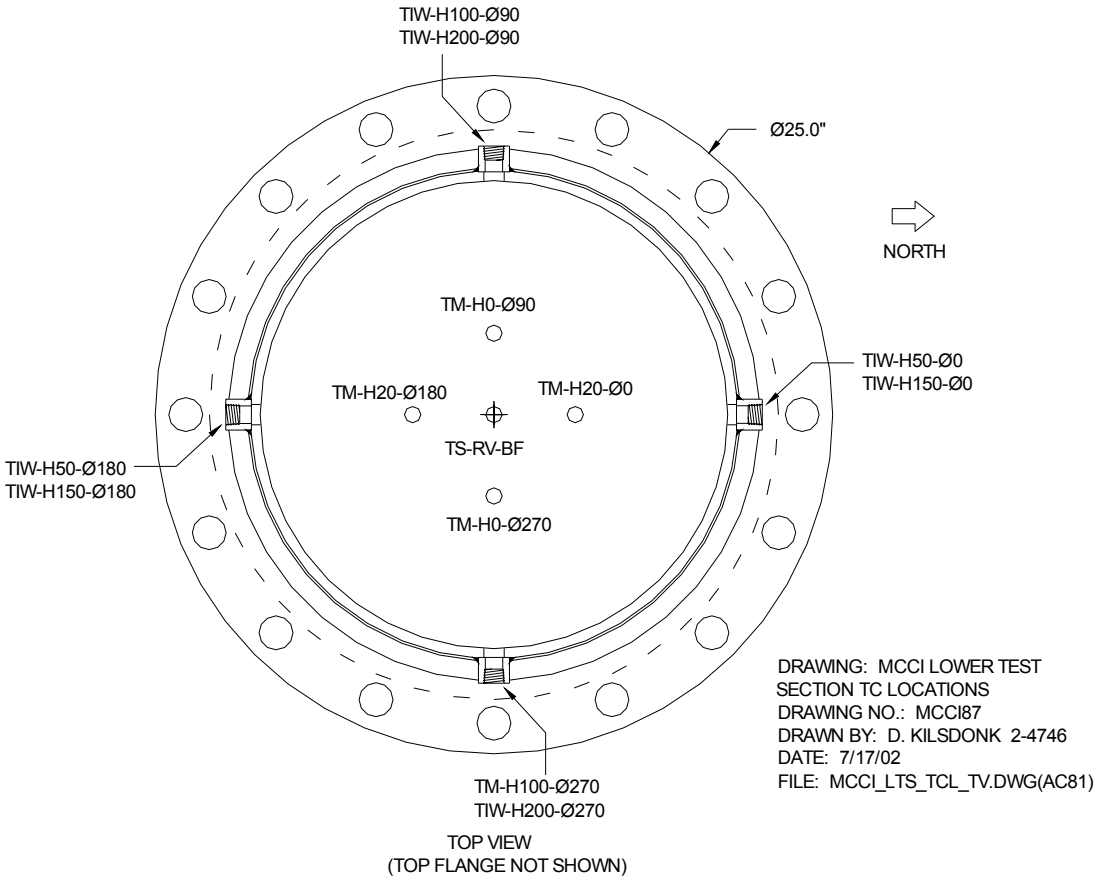

Figure 2.3 Reaction vessel thermocouple locations.

bottom of the melt, in mm, ϕ# (angle relative to direction north, in degrees). For example, TIW-50-ϕ180 is located at the inner wall of the MgO insulation, 50 mm above the bottom of the melt and south of the RV axis. Note that the four thermocouples penetrating the basemat are 76 mm from the RV centerline.

There are a total of eight locations near the base of the RV for radial instrument penetrations. One is reserved for a pyrometer to measure melt temperature at a level of 100 mm above the bottom of the melt. The pyrometer measures the temperature at the end of a tungsten thermowell (203 mm total length, 9.5 mm o.d.) that extends 50 mm from the MgO inner wall, into the melt.

Five of the remaining seven penetrations were used for thermocouples positioned at the outer edge of the melt to determine whether water seeps between the MgO wall and the crust as it forms above the melt. Though such seepage is deemed unlikely, this must be verified because the dryout heat flux measurement would be compromised by a melt that was partially cooled by water circumventing the crust. The remaining two instrument penetrations, located 200 mm above the bottom of the melt, were not used because they are about 50 mm above the expected top of the melt and thus would not yield any useful information.

#	Channel	Name	Type	Description	Serial #	Output	Range	Accuracy
0	HPS-0	T-CJ-HPS	AD592 IC	Cold junction compensation sensor.	-	1μA/K	0-70°C	± 0.5°C
1	HPS-1	TM-H0-ϕ90	TC type C	Melt temp. at bottom of melt.	-	0-37 mV	0-2320°C	± 4.5°C or 1%
2	HPS-2	TM-H0-ϕ270	TC type C	Melt temp. at bottom of melt.	-	0-37 mV	0-2320°C	± 4.5°C or 1%
3	HPS-3	TM-H20-ϕ0	TC type C	Melt temp. 20 mm above bottom of melt.	-	0-37 mV	0-2320°C	± 4.5°C or 1%
4	HPS-4	TM-H20-ϕ180	TC type C	Melt temp. 20 mm above bottom of melt.	-	0-37 mV	0-2320°C	± 4.5°C or 1%
5	HPS-5	TIW-H50-ϕ0	TC type C	Melt temp. at inner sidewall 50 mm above bottom of melt.	-	0-37 mV	0-2320°C	± 4.5°C or 1%
6	HPS-6	TIW-H50-ϕ180	TC type C	Melt temp. at inner sidewall 50 mm above bottom of melt.	-	0-37 mV	0-2320°C	± 4.5°C or 1%
7	HPS-7	TIW-H100-ϕ90	TC type C	Melt temp. at inner sidewall 100 mm above bottom of melt.	-	0-37 mV	0-2320°C	± 4.5°C or 1%
8	HPS-8	TIW-H150-ϕ0	TC type C	Melt temp. at inner sidewall 150 mm above bottom of melt.	-	0-37 mV	0-2320°C	± 4.5°C or 1%
9	HPS-9	TIW-H150-ϕ180	TC type C	Melt temp. at inner sidewall 150 mm above bottom of melt.	-	0-37 mV	0-2320°C	± 4.5°C or 1%
10	HPS-10	TOW-H100-ϕ90	TC type K	Melt temp. at outer sidewall 100 mm above bottom of melt.	-	0-50 mV	0-1250°C	± 2.2°C or 0.75%
11	HPS-11	TOW-H100-ϕ270	TC type K	Melt temp. at outer sidewall 100 mm above bottom of melt.	-	0-50 mV	0-1250°C	± 2.2°C or 0.75%
12	HPS-12	TG-RV	TC type C	Gas temp. in reaction vessel upper plenum.	-	0-37 mV	0-2320°C	± 4.5°C or 1%
13	HPS-13	TS-RV-300	TC type E	Outer wall temp. of RV 300 mm above bottom of melt.	-	0-70 mV	0-900°C	± 1.7°C or 0.5%
14	HPS-14	TS-RV-1000	TC type E	Outer wall temp. of RV 1000 mm above bottom of melt.	-	0-70 mV	0-900°C	± 1.7°C or 0.5%
15	HPS-15	TS-RV-tf	TC type E	Temperature of RV top flange	-	0-70 mV	0-900°C	± 1.7°C or 0.5%
16	HPS-16	TS-vent	TC type E	Outer wall temp. of vent line.	-	0-70 mV	0-900°C	± 1.7°C or 0.5%
17	HPS-17	TS-RV-bf	TC type K	Temperature of RV bottom flange.	-	0-50 mV	0-1250°C	± 2.2°C or 0.75%
18	HPS-32	TS-RV-50	TC type K	Outer wall temp. of RV 50 mm above bottom of melt.	-	0-50 mV	0-1250°C	± 2.2°C or 0.75%
19	HPS-18	TF-CT-102	TC type K	Fluid temp. in condensate tank at a water level of 102 mm.	-	0-50 mV	0-1250°C	± 2.2°C or 0.75%
20	HPS-19	TF-CT-406	TC type K	Fluid temp. in condensate tank at a water level of 406 mm.	-	0-50 mV	0-1250°C	± 2.2°C or 0.75%
21	HPS-20	TF-CT-711	TC type K	Fluid temp. in condensate tank at a water level of 711 mm.	-	0-50 mV	0-1250°C	± 2.2°C or 0.75%
22	HPS-21	TF-CT-1016	TC type K	Fluid temp. in condensate tank at a water level of 1016 mm.	-	0-50 mV	0-1250°C	± 2.2°C or 0.75%
23	HPS-22	TF-CT-1321	TC type K	Fluid temp. in condensate tank at a water level of 1321 mm.	-	0-50 mV	0-1250°C	± 2.2°C or 0.75%
24	HPS-23	TF-CT-1626	TC type K	Fluid temp. in condensate tank at a water level of 1626 mm.	-	0-50 mV	0-1250°C	± 2.2°C or 0.75%
25	HPS-24	TF-HX-in	TC type K	Fluid temp. at HX coolant inlet.	-	0-50 mV	0-1250°C	± 2.2°C or 0.75%
26	HPS-25	TF-HX-out	TC type K	Fluid temp. at HX coolant outlet.	-	0-50 mV	0-1250°C	± 2.2°C or 0.75%
27	HPQ-51	TF-ST	TC type K	Fluid temp. in spray tank.	-	0-50 mV	0-1250°C	± 2.2°C or 0.75%
28	HPQ-53	TG-ST-in	TC type K	Gas temp. in the spray tank line inlet.	-	0-50 mV	0-1250°C	± 2.2°C or 0.75%
29	HPQ-54	TG-ST-out	TC type K	Gas temp. in the spray tank line outlet.	-	0-50 mV	0-1250°C	± 2.2°C or 0.75%
30	HPS-26	HF-RV-300	Thermopile	Heat Flux through RV wall 300 mm above bottom flange.	0629	0-5.72 mV	0-5 kW/m^2	± 3%
31	HPS-27	HF-RV-1000	Thermopile	Heat Flux through RV wall 1000 mm above bottom of flange.	0630	0-5.19 mV	0-5 kW/m^2	± 3%
32	HPS-28	HF-RV-tf	Thermopile	Heat Flux through RV top flange.	0631	0-5.56 mV	0-5 kW/m^2	± 3%
33	HPS-29	HF-vent	Thermopile	Heat Flux through connecting line to V-ST.	0632	0-5.50 mV	0-5 kW/m^2	± 3%
34	HPS-30	TM-H100-ϕ270	Pyrometer	Melt temp. 50 mm from sidewall, 100 mm above bottom of melt.	-	4-20 mA	1200-3000°C	± 0.3%
35	HPS-31	I-ign	DC supply	Current supply for thermite ignitor.	-	0-100 mV	0-25 Amps	-
36	HPS-33	PA-RV	1810AZ	Absolute pressure in reaction vessel.	2	0-12 V	0-4 bar	± 0.03 bar

Table 2.1 Instrumentation list (part 1 of 2).

#	Channel	Name	Type	Description	Serial #	Output	Range	Accuracy
37	HPS-34	PD-RV	1801DZ	ΔP: Atmospheric pressure - pressure 450 mm above bottom of melt.	D-2	0-13 V	0-0.35 bar	A 0.004 bar
38	HPS-35	PD1-CT	1801DZ	ΔP transmitter to measure condensate inventory.	D-9	0-13 V	0-0.35 bar	A 0.004 bar
39	HPS-36	PD2-CT	1801DZ	ΔP transmitter to measure condensate inventory.	D-4	0-13 V	0-0.35 bar	A 0.004 bar
40	HPS-37	VDC-P-supply	-	Voltage of the power supply for the pressure transmitters.	-	0-15 V	-	-
41	HPQ-50	T-CJ-HPQ	AD592 IC	Cold junction compensation sensor.	-	1μA/K	0-70°C	A 0.5°C
42	HPQ-52	TG-CL-out	TC type K	Gas temperature in condensate tank outlet line to spray tank.	-	0-50 mV	0-1250°C	A 2.2°C or 0.75%
43	HPQ-55	F-quench	Paddlewheel	Flow rate of cold water to heat exchangers.	3143	0-5 V	0-50 gpm	A 0.5 gpm
44	HPQ-56	F-HX	Paddlewheel	Flow rate of water into reaction vessel (for quenching melt).	3180	0-5 V	0-18 gpm	A 0.18 gpm

Table 2.2 Instrumentation list (part 2 of 2).

Channel #		Valve Name	Type	Description	Actuator
1		V-CT	Ball valve	Valve on steam line between reaction vessel and quench tank.	Pneumatic
2		V-quench	Ball valve	Valve on quench water supply line into reaction vessel.	Solenoid
3		V-H2O-i	Ball valve	Isolation valve on quench water supply line into reaction vessel.	Solenoid
4		V-H2O-b	Ball valve	Bypass valve on quench water supply line into reaction vessel.	Solenoid
5		V-ST	Ball valve	Valve on vent line between reaction vessel and spray tank.	Pneumatic
-		V-HX	Ball valve	Valve on cooling-water line to heat exchangers.	Solenoid

Table 2.3 Remotely operated valves.

Parameter	SSWICS-1	SSWICS-2	SSWICS-3
Test section internal diameter (cm)	30.5	30.5	30.5
Melt composition (wt % UO_2/ZrO_2/Cr/Concrete)	61/25/6/8	61/25/6/8	TBD*
Concrete type	LCS	SIL	TBD
Melt mass at maximum depth (kg)	75	75	TBD
Initial Melt Temperature (°C)	~2200	~2200	TBD
Basemat type	Inert	Inert	Inert
System pressure (bar)	1	1	3
Water injection flowrate (lpm)	8.4	8.4	8.4
Water depth (cm)	50	50	50

Table 3.1 Test specifications for the first three SSWICS experiments.

Constituent	Mass (kg)
U_3O_8	47.54
CrO_3	8.53
CaO	0.94
Zr	13.90
Mg	0.03
Si	0.75
SiO_2	3.17
Al	0.15
Total	75.0

Constituent	Wt %	
	Reactant	Product
U_3O_8	63.38	-
UO_2	-	60.97
Zr	18.53	-
ZrO_2	-	25.04
Si	1.00	-
SiO_2	4.23	6.38
Mg	0.04	-
MgO	-	0.07
Al	0.20	-
Al_2O_3	-	0.38
CaO	1.25	1.25
CrO_3	11.37	-
Cr	-	5.91

Tables 3.2 Corium powder charge and reaction product mass fractions.

Four heat flux meters are used to obtain direct measurements of local heat losses. Two sensors were attached to the side of the RV, a third to the top flange, and the fourth is mounted to the 4" vent line between the RV and valve V-ST. The entire RV was insulated from the melt level upwards. Though the insulation around the upper plenum should ensure that heat losses are small compared to the heat transfer rate through the cooling coils, the heat flux sensors provide an added reduction in uncertainty in the energy balance used to calculate heat flux from the corium melt. The lower 25 cm of the RV was left uninsulated so that any excessive wall heating or corium breach can be readily observed.

3. Test Parameters and Course of Test

The specifications for this test are listed in table 3.1 along with those for the first and third tests for comparison. The measured masses of the constituents of the corium powder charge are listed in table 3.2. The 75 kg charge was selected to produce an approximate melt depth of 15 cm.

Shortly before thermite ignition, the valves were positioned so that ignition gases would be vented directly into the spray tank (i.e., valve V-ST open and valve V-CT closed). The helium gas flow of 10 slpm, which had been used to maintain an inert atmosphere within the reaction vessel during the 4 days since the charge was loaded, was switched to the vent line (see fig. 2.2). Water flow to the heat exchanger was set at 42 l/min.

The igniter coils were energized to initiate thermite ignition and, after twenty seconds, the upper plenum gas temperature TG-RV began to increase. Thermocouples within the melt began rising about twenty seconds later. The signal from the igniter has not been included in any graph in this report, but all data has been plotted with the initial signal to the igniter as the x-axis origin.

The melt thermocouples TM-H20-ϕ0 and TM-H20-ϕ90 rose rapidly to an initial peak temperature of 2210 and 2290^{o}C, respectively, before dropping and holding a plateau for several minutes at about 1800^{o}C. Both temperatures then rose so that eight minutes after ignition they were near 2100^{o}C. Figure A.1 shows the first fifteen minutes of the transient (all plots are attached as an appendix). The pyrometer indicated a peak temperature of 2140^{o}C.

The next phase of the experiment was the initial quench of the melt. Valve V-CT was opened 80 s after ignition so that steam would be able to travel to the heat exchangers. Valve V-ST was closed at 100 s to isolate the vent line and spray tank from the system. Water injection was initiated at 140 s at a flow rate of 3.2 l/min, lasting for 12.7 minutes (ending at 900 s) and resulting in an integrated flow of approximately 39 liters.

The plots of RV structure temperatures show the upper sidewalls rising to the saturation temperature within 500 s. The top and bottom flanges heated more slowly than the RV walls. The temperature of the top flange dipped during the injection phase and did not rise towards the saturation temperature until after water injection ceased.

The pyrometer exhibited a smooth decline in temperature after the initial peak. The sensor reached its lower range limit of 1200^{o}C 27 minutes after ignition.

4. Sensor Malfunctions and Abnormalities

Post test examination of the test apparatus and a preliminary review of the data indicate the following:

1) Sensor TM-H20-ϕ180 failed at 1845 s and TM-H20-ϕ0 failed at 2390 s.
2) The measured temperatures at the inner wall of the MgO insulation did not exhibit the orderly decrease that was observed during the first test. It was expected that the thermocouples at higher elevations would drop to the saturation temperature before those at lower elevations. In addition, the temperatures were expected to decrease nearly monotonically, which was not the behavior of sensors TIW-H50-ϕ180 and TIW-H100-ϕ90. It is believed that, rather than an indication of water penetration between the corium and the MgO, the data suggests that the thermocouples were not properly sealed on the outside of the MgO liner, allowing water to come close to the sensor tip through the hole in the liner. For future tests, the thermocouple penetrations will be filled with a special sealing compound to prevent water/steam ingression near the thermocouple tips.

5. Data Reduction

Some simple calculations have been performed to provide a preliminary assessment of the test data. The first is a calculation of the coolant inventory in the RV as a function of time. The inventory is the difference between the total amount of liquid injected and the amount boiled off and collected in the CT:

$$M_{H_2O-RV} = \sum_{t=0}^{t=t_{end}} \rho \dot{V} \Delta t \quad - \quad \frac{\pi}{4} D^2 \frac{\Delta P}{g} \tag{5.1}$$

where data from sensor F-quench is used for the volumetric flow rate $\dot{V}$ and the liquid density ρ is taken to be 998 kg/m^3. The condensate inventory is calculated with readings from sensor PD2-CT (ΔP) and the tank diameter D of 0.203 m. Figure A.7 shows both the integrated mass flow and CT inventory, labeled F-integrated and M- CT, respectively. The calculated net coolant inventory, denoted M-RV, confirms that the corium was always covered with water.

The corium heat flux was calculated using two different methods. The first considers the rate of condensate collection, which is a measure of the steam flow rate from the RV. Accurate determination of the heat flux at the corium surface must, however, account for various heat sinks. During the injection phase, energy is absorbed raising the coolant to the saturation temperature. Some of the vapor produced by the quenching melt condenses on the walls of the upper plenum to heat the RV structures to the saturation temperature. Later, heat losses from the upper plenum generate continued condensation. Accounting for these heat sinks, the rate of energy transfer through the corium surface is written as:

$$Q = M_{RV}\, c_p \frac{\partial T}{\partial t} + \dot{m}\, h_{fg} + \left[M_S c_M \frac{\partial T}{\partial t} + Q_{HL} \right] \Bigg|_{up} \tag{5.2}$$

where $\dot{m}$ is mass flow rate of condensate into the CT, M_S is the mass of the RV upper plenum structures, c_M is their heat capacity,, and Q_{HL} represents total upper plenum heat losses. For this report, liquid subcooling has been neglected (an accurate assumption after the injection phase) along with heat losses and time variations in structure temperatures. The condensation rate is calculated from the time derivative of the differential pressure signal PD2-CT. The heat transfer rate from the corium is then:

$$Q = \frac{1}{g}\frac{\pi}{4}D^2\frac{\partial \Delta P}{\partial t}h_{fg} \tag{5.3}$$

where D is again the inner diameter of the CT and the heat of vaporization h_{fg} is 2257 kJ/kg^{o}C. The heat flux is obtained by scaling Q with the initial surface area of the corium (0.073 m^2). The derivative was calculated with pairs of averaged ΔP readings (an average of 5 measurements at 0.5 Hz) centered around a Δt of 60 s. The averaging and length of Δt were necessary to reduce oscillations in the calculated heat flux.

The second method of calculating corium heat flux uses an energy balance on the secondary side of the heat exchanger. The measured parameters are the coolant flow rate on the secondary side of the cooling coils and the inlet and outlet coolant temperatures. The cooling power of the heat exchanger is then:

$$Q_{HX} = \rho \dot{V}_{HX}\, c_p \left(T_{out} - T_{in}\right) \tag{5.4}$$

where readings from sensors TF-HX-in and TF-HX-out were used for temperatures T_{in}, and T_{out}, respectively. Data from the flow meter F-HX was used for $\dot{V}_{HX}$ and the density of water was again taken to be 998 kg/m^3.

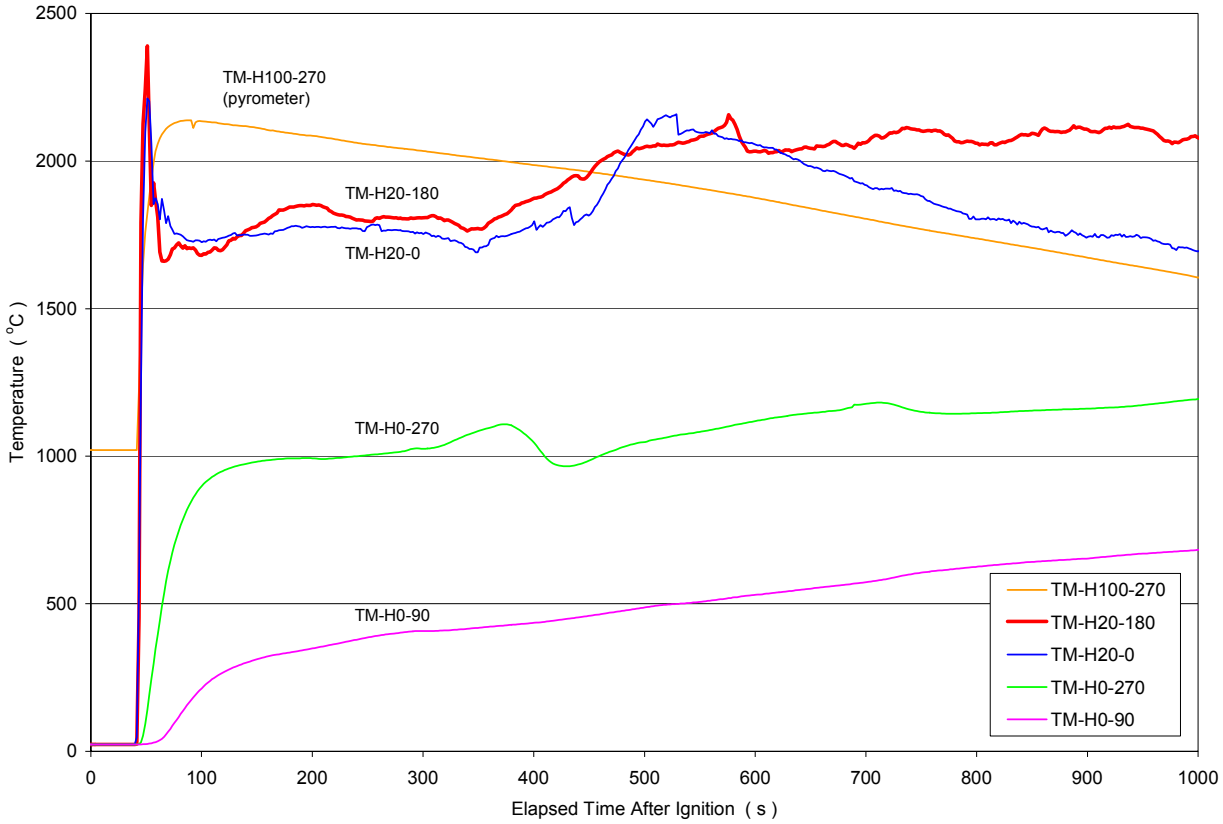

Figure A.1 Melt temperatures early in the transient.

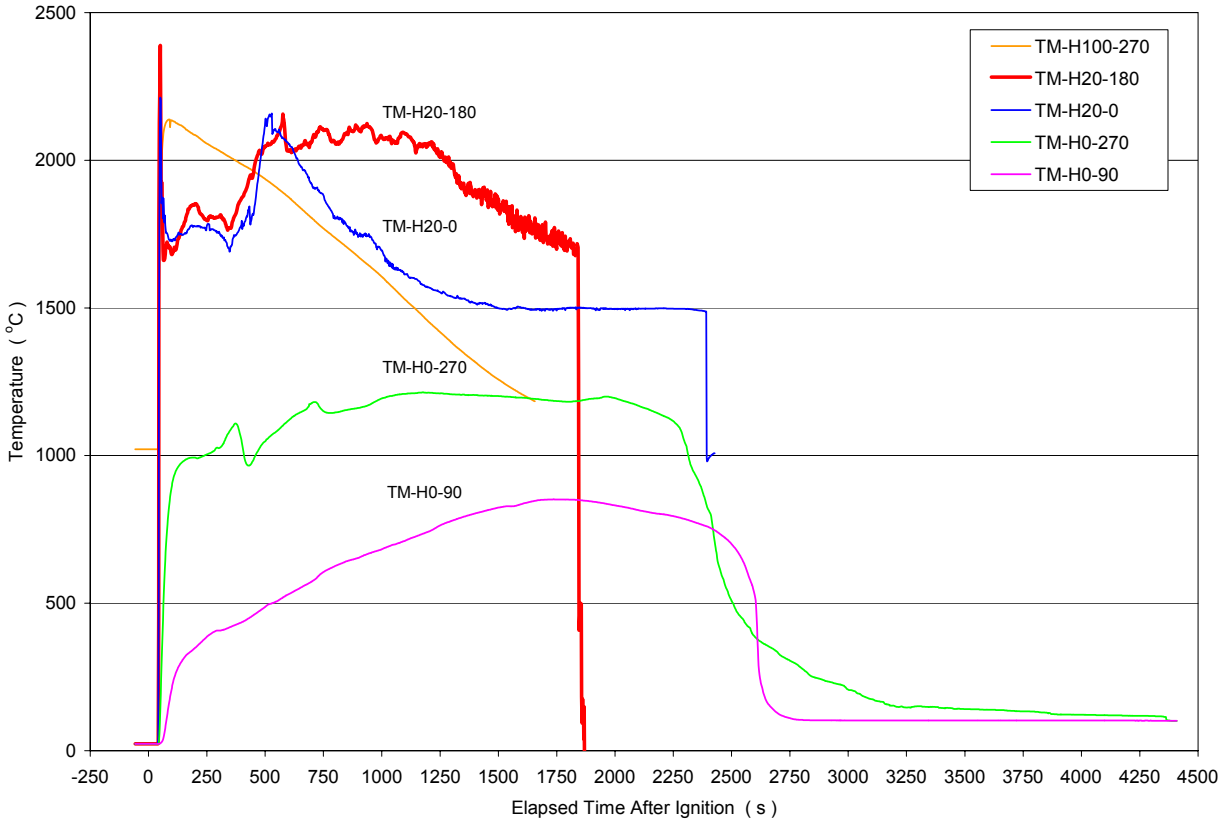

Figure A.2 Melt temperatures for the entire test duration.

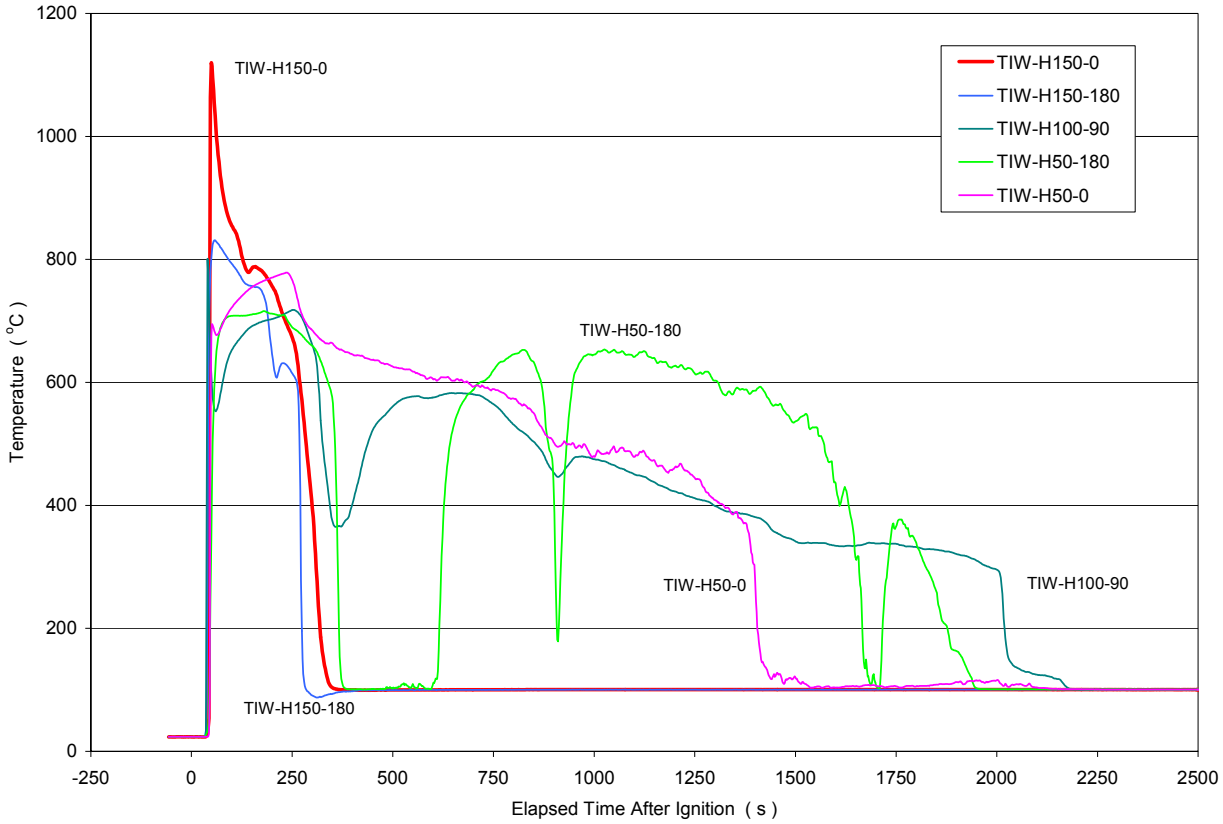

Figure A.3 Temperatures at the inner wall of MgO insulator.

Figure A.4 Structure temperatures.

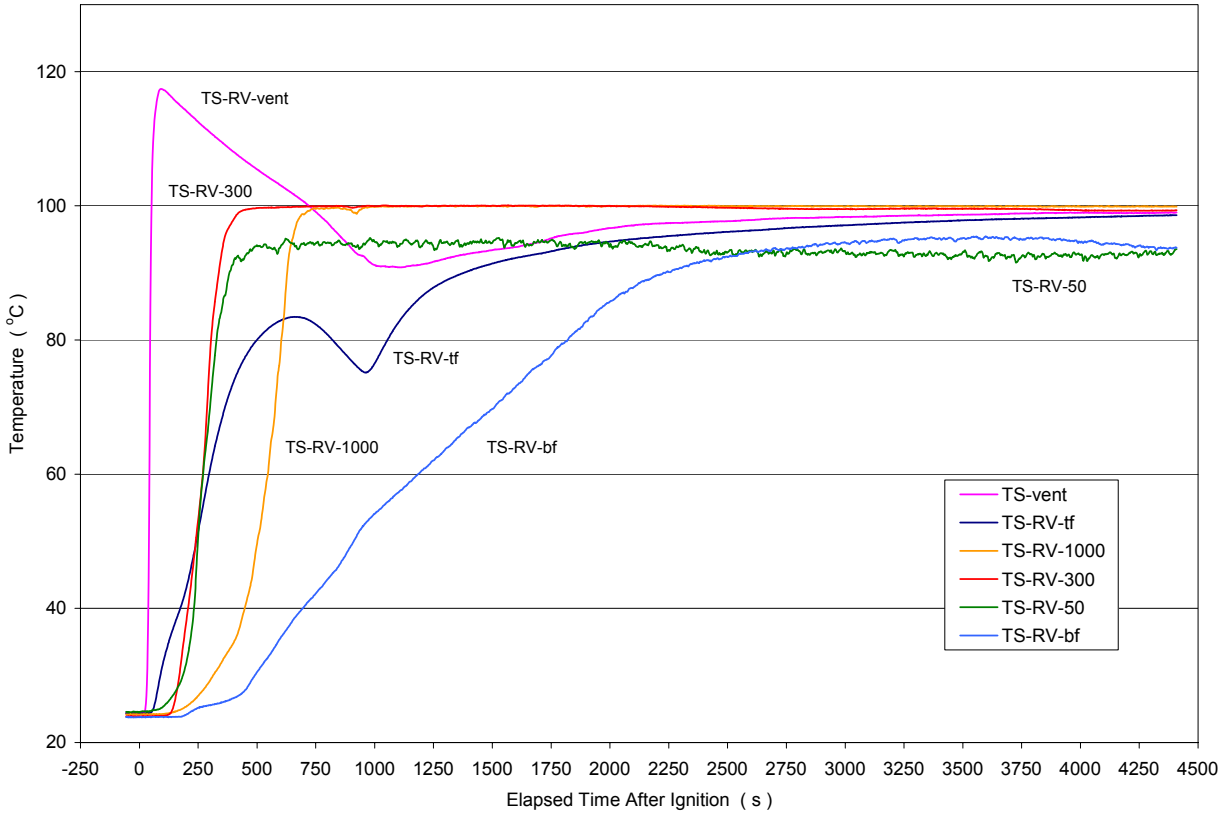

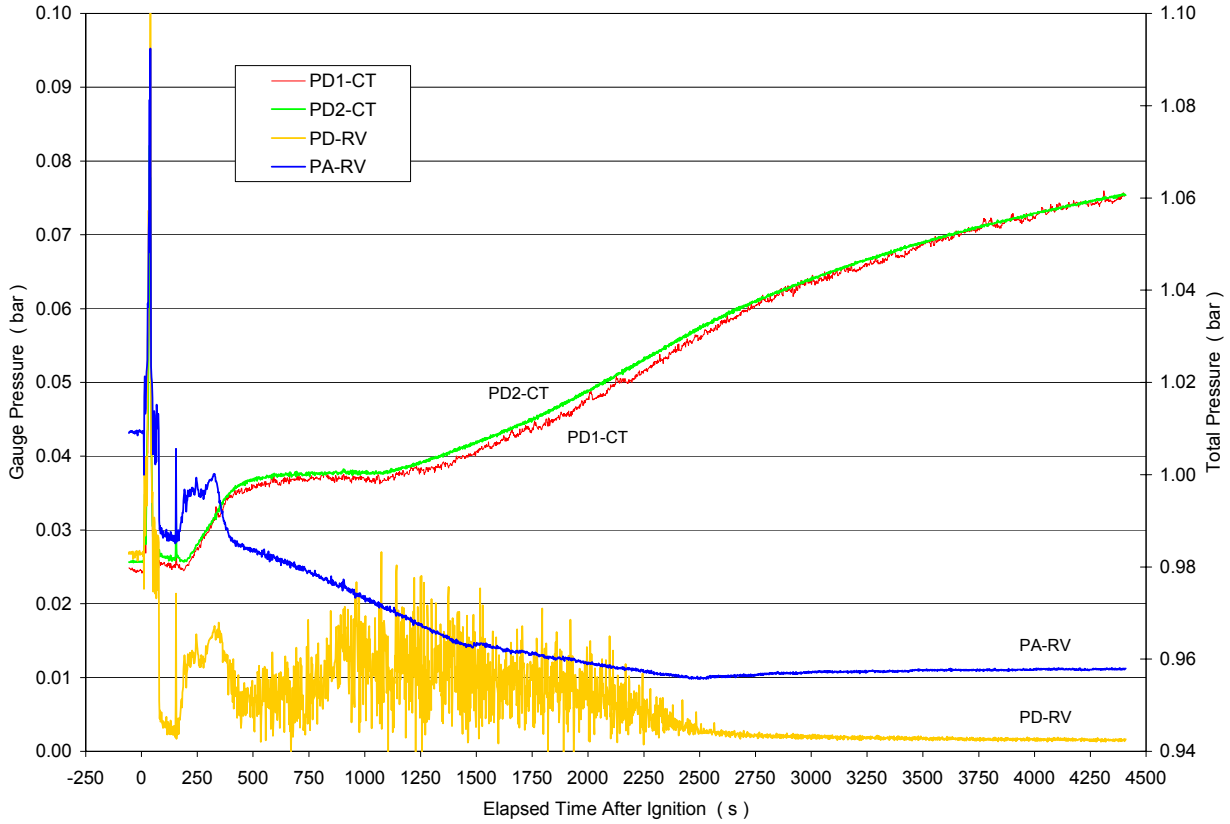

Figure A.5 Pressure and ΔP in RV and condensate tank.

Figure A.6 Water injection into RV and HX secondary side flow rate.

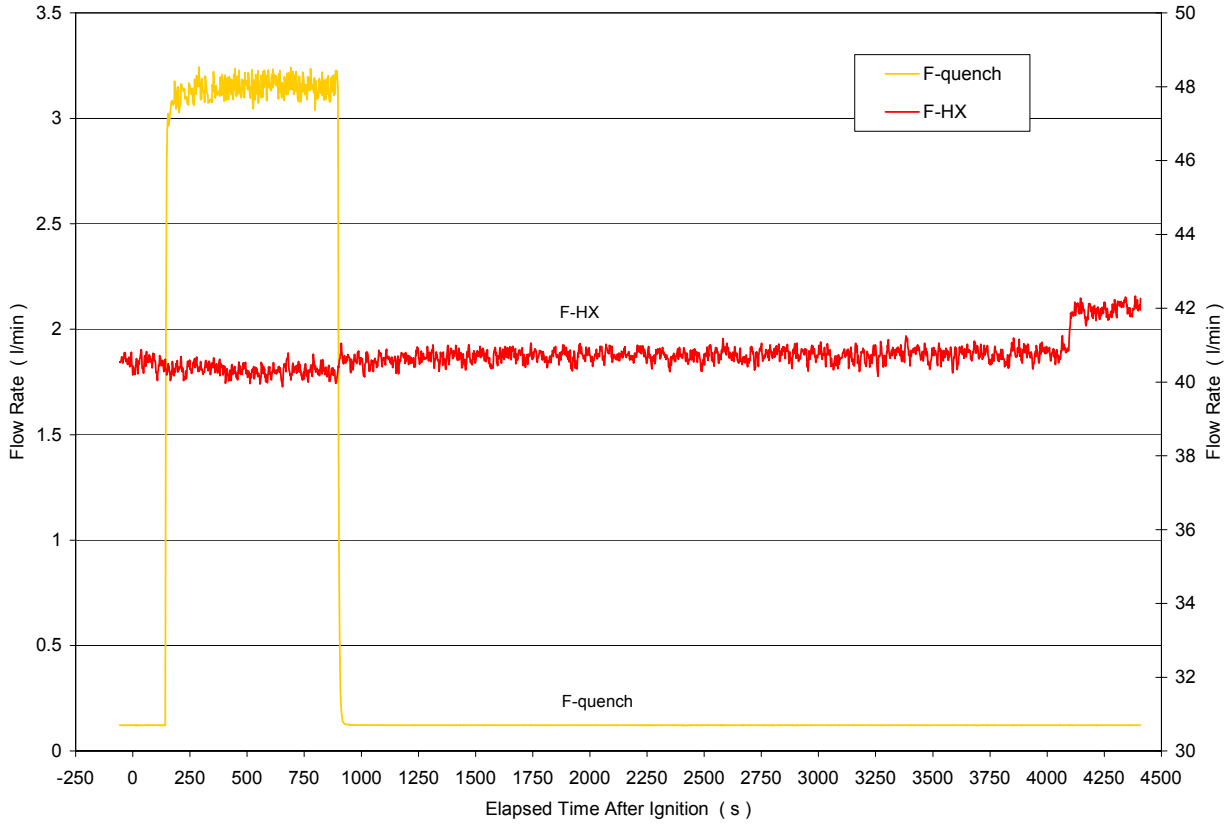

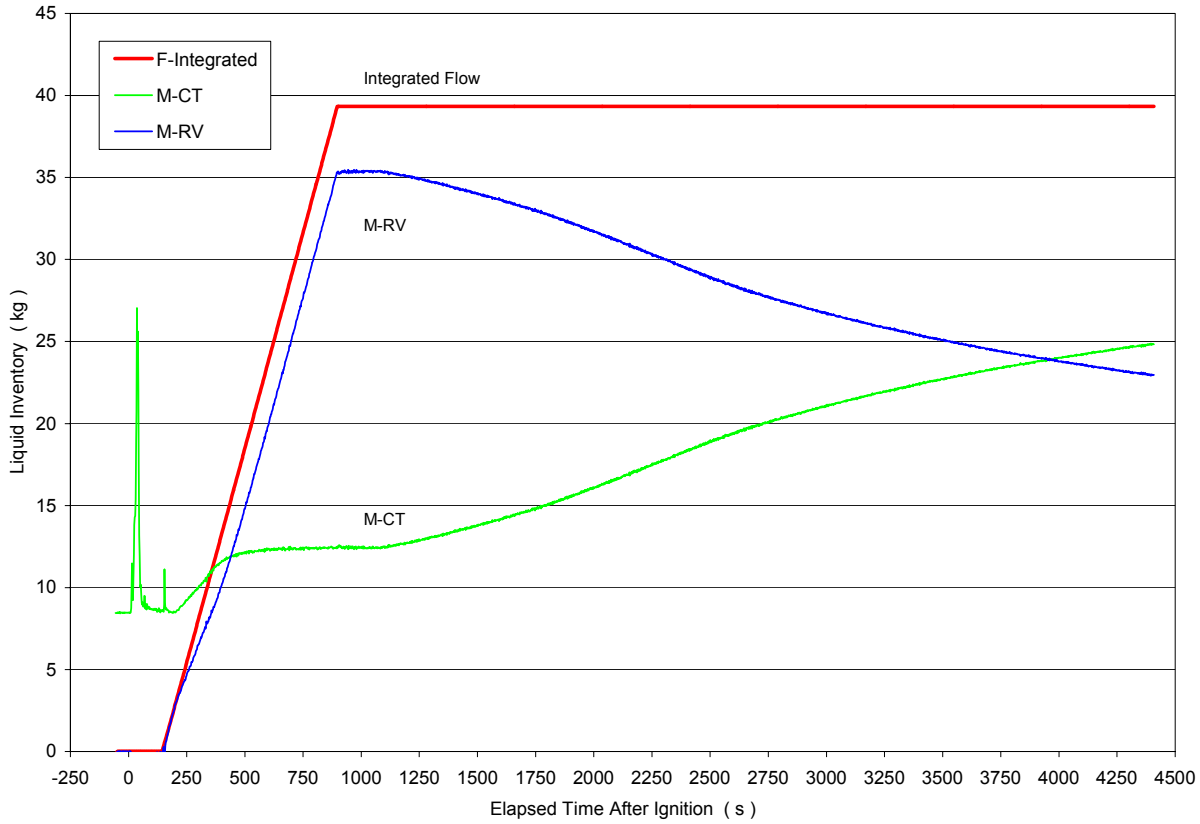

Figure A.7 Integrated quench flow and calculated RV liquid inventory.

Figure A.8 Secondary side fluid temperatures at HX inlet and outlet.

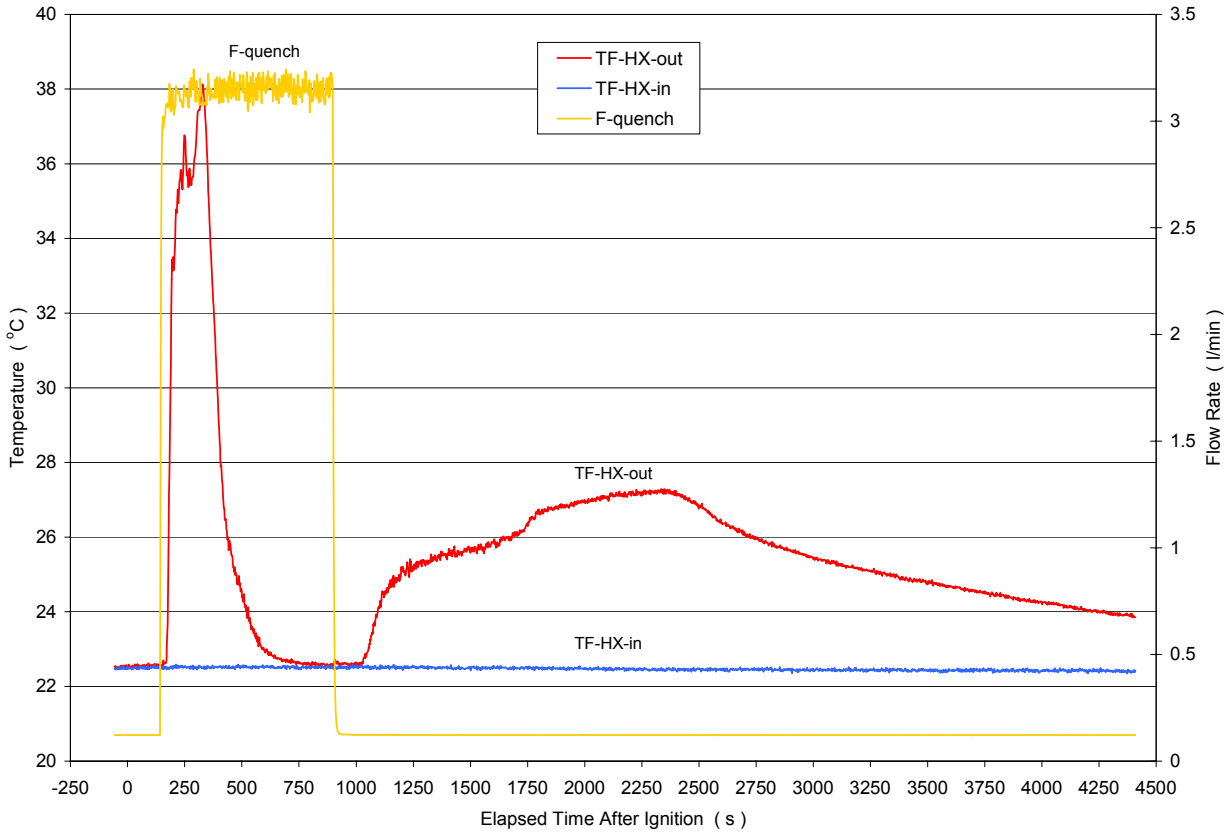

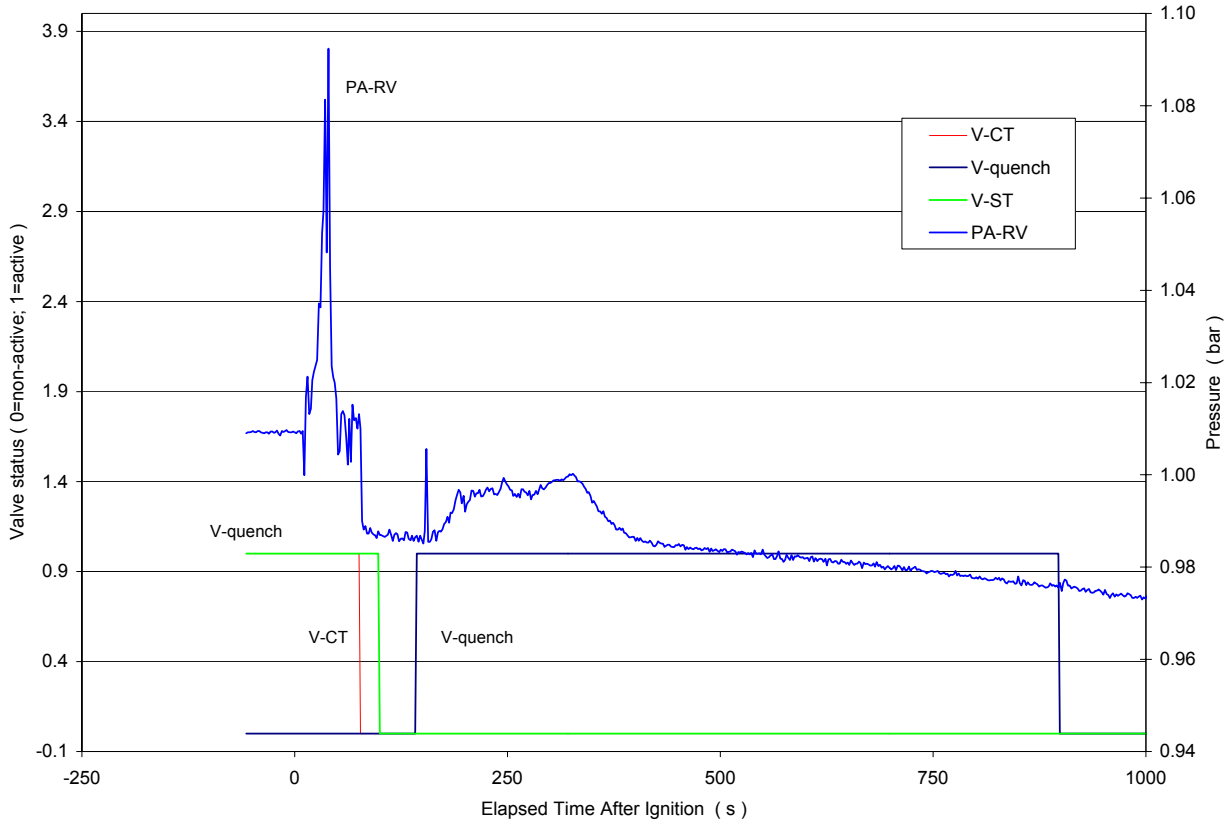

Figure A.9 Valve status during course of test.

Figure A.10 Measured heat flux at RV and vent line surfaces.

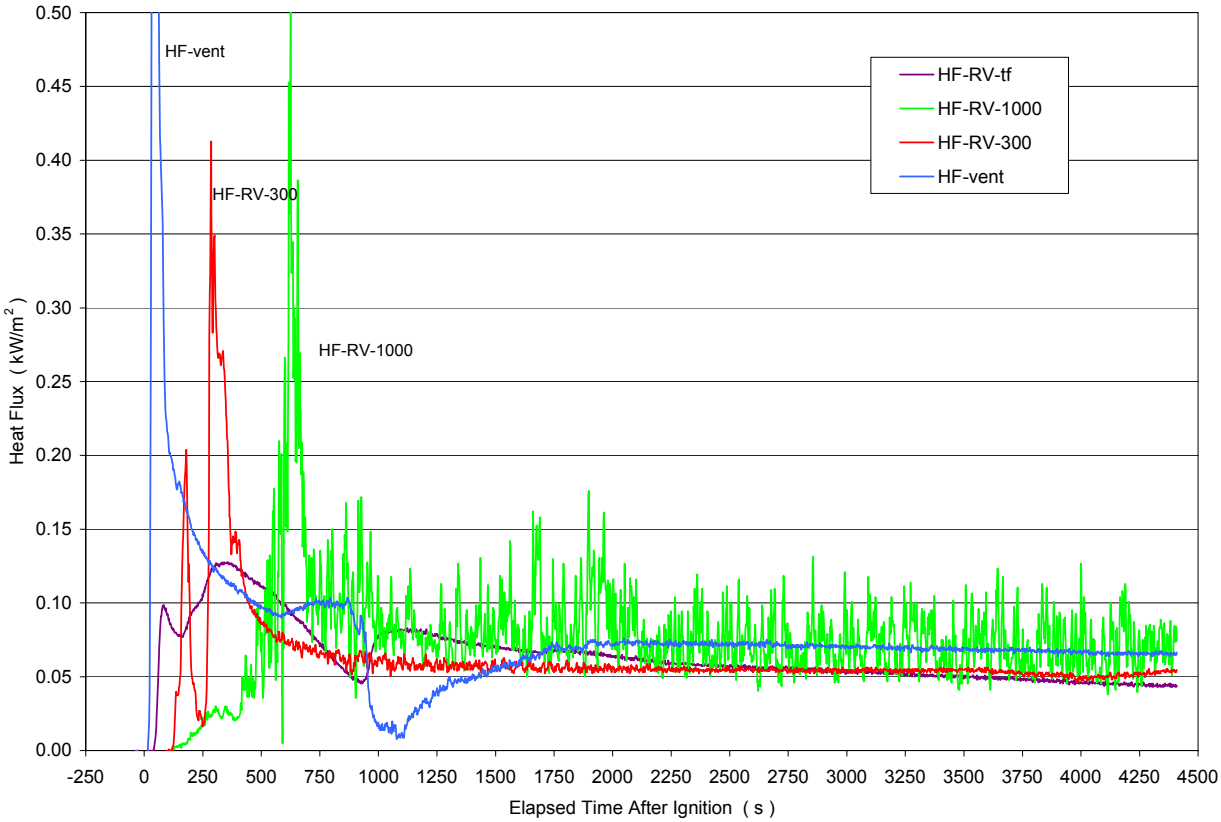

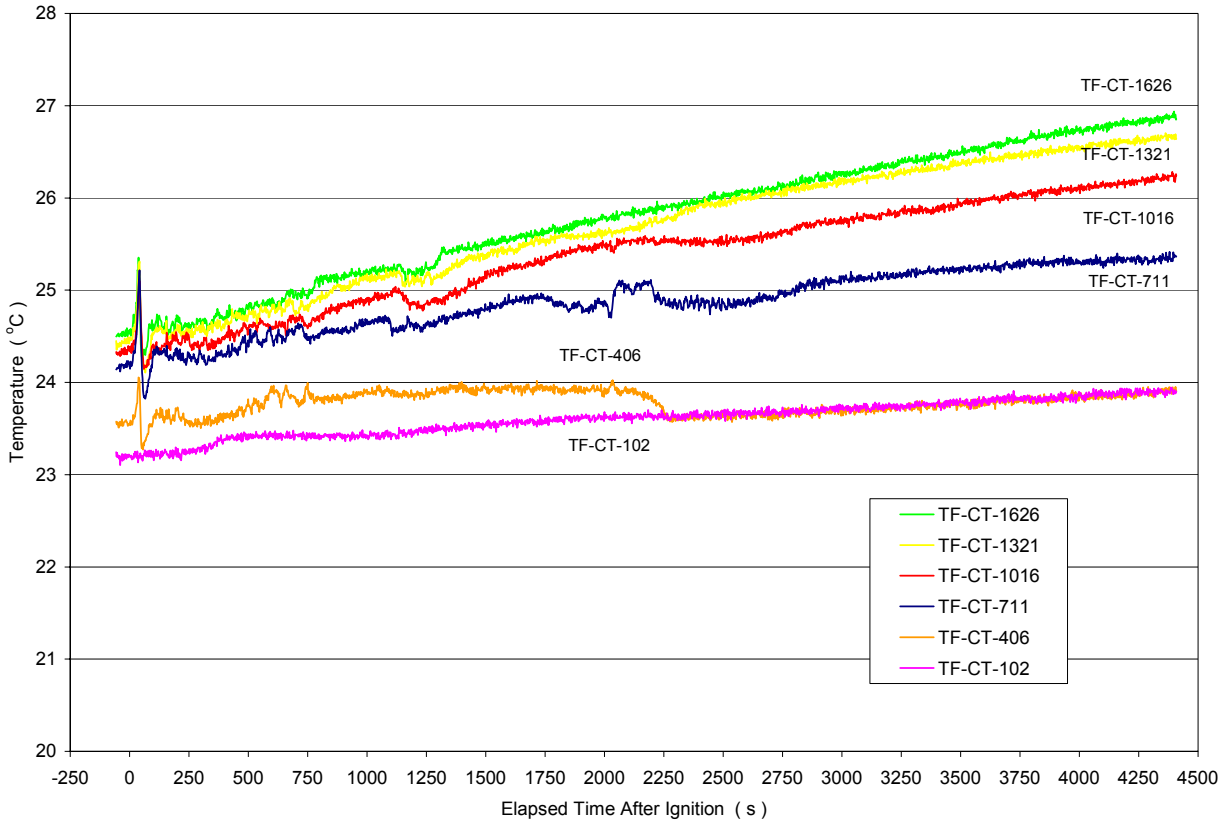

Figure A.11 Fluid temperatures in the condensate tank.

Figure A.12 Calculated heat flux through corium.